# Support information

**Constructing a highly functional oxygen defects Li$_7$La$_3$Zr$_2$O$_{12}$-polyacrylonitrile composite electrolytes for all-solid-state lithium-ion batteries**

Hualing Tian,[a,b] Yanhui Zhang,[a,b] Yanjun Cai,[a,b,*] Xiang Yao[a,b] and Zhi Su[a, b,c,*]

[a] College of Chemistry and Chemical Engineering, Xinjiang Normal University, Urumqi, 830054, Xinjiang, China. E-mail: cyjxjsf@yeah.net, suzhixj@sina.com.

[b] Xinjiang Key Laboratory of Energy Storage and Photoelectrocatalytic Materials, Urumqi, 830054, Xinjiang, China.

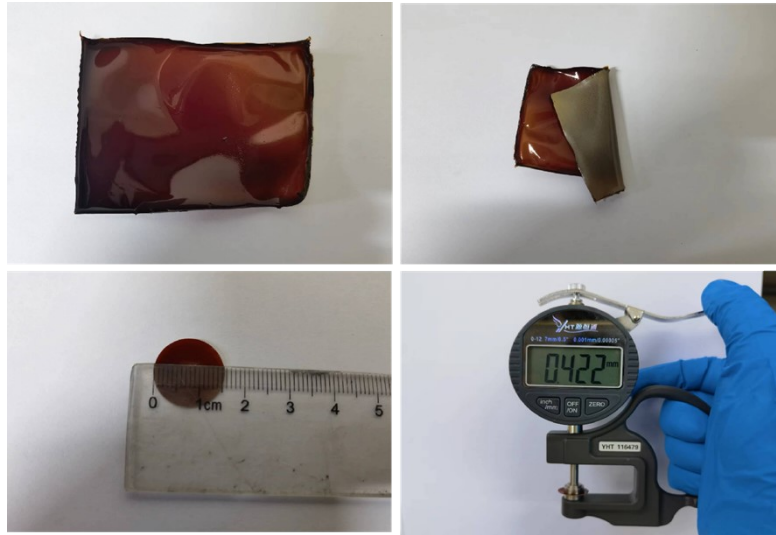[c] Xinjiang Institute of Technology, China.
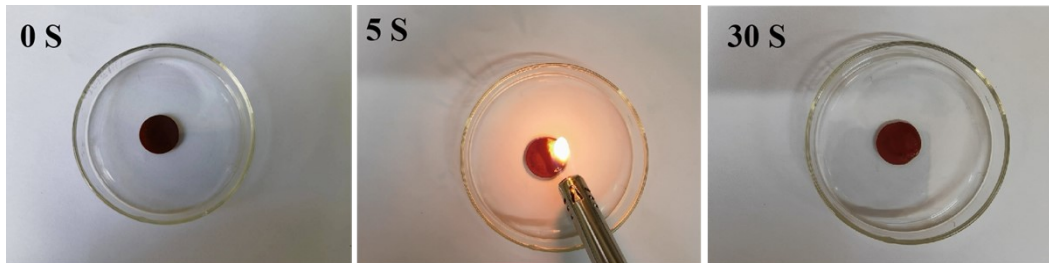
Fig. S1 The optical image of LLZO-PAN membrane



Fig. S2 LLZO-PAN fire resistance test

Table S1 Lattice parameters for the preparation of LLZO samples

| samples | lattice constants (Å³) | lattice constants (Å³) |
|---------|------------------------|------------------------|
| LLZO-0 | 17.4895 | 11.1916 |
| LLZO-1 | 17.6514 | 11.0358 |
| LLZO-2 | 18.0013 | 10.6009 |
| LLZO-3 | 17.8962 | 10.4966 |

Table S2 The components of LLZO-0 material

| Chemical Formula | LLZO-0 | $Li_{0.5}La_2Al_{0.5}O_4$ | $LaAlO_3$ | $La_2O_3$ | $La_2Zr_2O_7$ |
|------------------|--------|---------------------------|-----------|-----------|----------------|
| quantity contained (%) | 77.8 | 11.9 | 3.3 | 3.9 | 3.1 |

Table S3 The components of LLZO-2 material

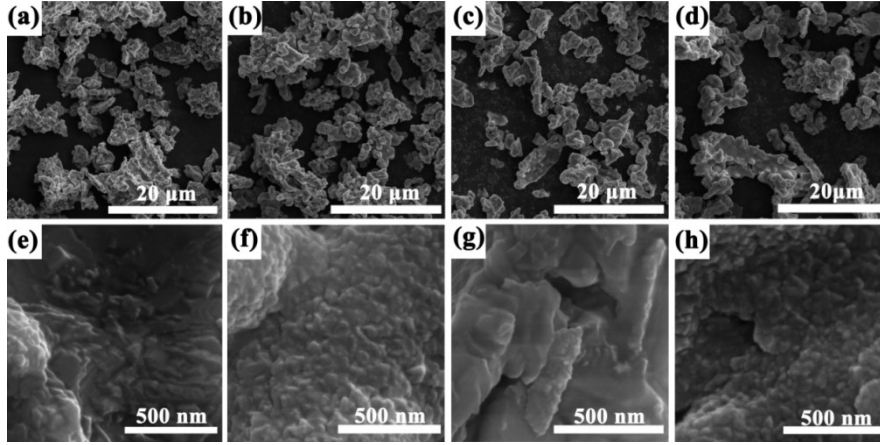| Chemical Formula | LLZO-2 | $Li_{0.5}La_2Al_{0.5}O_4$ | $LaAlO_3$ | $La_2O_3$ | $La_2Zr_2O_7$ |
|------------------|--------|---------------------------|-----------|-----------|----------------|
| quantity contained (%) | 73.5 | 13.1 | 0.99 | 7.31 | 5.1 |

Fig. S3 SEM images of LLZO materials (a, e) LLZO-0, (b, f) LLZO-1, (c, g) LLZO-2, (d, h) LLZO-3.

The effects of oxygen vacancies on the electrochemical performance of composite electrolyte LLZO-PAN at optimal condition were investigated. Ionic conductivities of the SSEs were measured using electrochemical impedance spectroscopy (EIS) with SS|LLZO-PAN |SS (SS, stainless steel), under frequency ranging from 0.1 Hz to $10^5$ Hz. Ionic conductivity was calculated using Eq. (S1):

$$\sigma = d/RS \qquad (S1)$$

where $d$ is thickness of the composite electrolyte membrane, and $S$ is the effective electrode area ($S$ = 2.0096 cm$^2$). The corresponding intra-grain ($R_g$) and inter-grain ($R_{gb}$) resistances were obtained by modeling the equivalent EIS circuit. The total resistance $R$ was the sum of $R_g$ and $R_{gb}$.


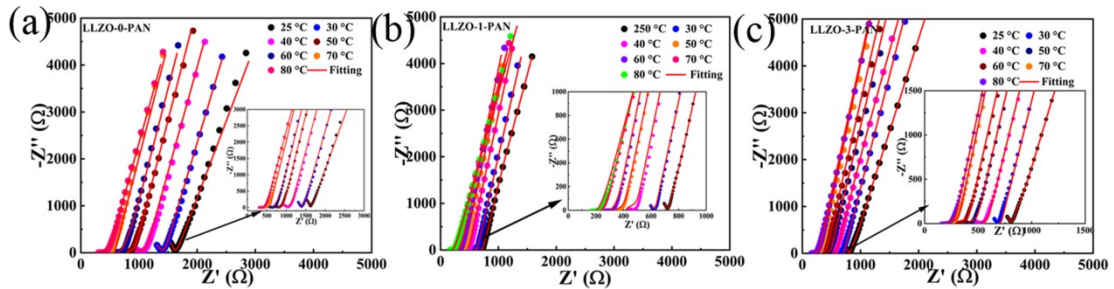
Fig. S4 Nyquist plots of (a) LLZO-0-PAN composite electrolyte, (b)LLZO-1-PAN composite electrolyte, (c) LLZO-3-PAN composite electrolyte.

Table S4 Ionic Conductivity of LLZO-0-PAN SSE

| T (°C) | d (cm) | $R_g$ (Ω) | $R_{gb}$ (Ω) | R (Ω) | σ ($R_g$)(S cm$^{-1}$) | σ ($R_{gb}$)(S cm$^{-1}$) | σ (R)(S cm$^{-1}$) |
|---|---|---|---|---|---|---|---|
| 25 | 6.03x10$^{-2}$ | 1005 | 556 | 1561 | 3.00×10$^{-5}$ | 5.42×10$^{-5}$ | 1.93×10$^{-5}$ |
| 30 | 6.03x10$^{-2}$ | 950 | 430 | 1380 | 3.17×10$^{-5}$ | 7.01×10$^{-5}$ | 2.18×10$^{-5}$ |
| 40 | 6.03x10$^{-2}$ | 913 | 380 | 1293 | 3.30×10$^{-5}$ | 7.93×10$^{-5}$ | 2.33×10$^{-5}$ |
| 50 | 6.03x10$^{-2}$ | 760 | 295 | 1055 | 3.97×10$^{-5}$ | 1.02×10$^{-4}$ | 2.86×10$^{-5}$ |
| 60 | 6.03x10$^{-2}$ | 620 | 150 | 770 | 4.86×10$^{-5}$ | 2.01×10$^{-4}$ | 3.92×10$^{-5}$ |
| 70 | 6.03x10$^{-2}$ | 580 | 140 | 720 | 5.20×10$^{-5}$ | 2.15×10$^{-4}$ | 4.19×10$^{-5}$ |
| 80 | 6.03x10$^{-2}$ | 360 | 110 | 470 | 8.38×10$^{-5}$ | 2.74×10$^{-4}$ | 6.41×10$^{-5}$ |

Table S5 Ionic Conductivity of LLZO-1-PAN SSE

| T (°C) | d (cm) | $R_g$ (Ω) | $R_{gb}$ (Ω) | R (Ω) | σ ($R_g$)(S cm$^{-1}$) | σ ($R_{gb}$)(S cm$^{-1}$) | σ (R)(S cm$^{-1}$) |
|---|---|---|---|---|---|---|---|
| 25 | 5.6x10$^{-2}$ | 510 | 260 | 770 | 4.59×10$^{-5}$ | 1.08×10$^{-4}$ | 3.64×10$^{-5}$ |
| 30 | 5.6x10$^{-2}$ | 465 | 200 | 665 | 6.02×10$^{-5}$ | 1.40×10$^{-4}$ | 4.21×10$^{-5}$ |
| 40 | 5.6x10$^{-2}$ | 410 | 160 | 570 | 6.83×10$^{-5}$ | 1.75×10$^{-4}$ | 4.91×10$^{-5}$ |
| 50 | 5.6x10$^{-2}$ | 370 | 125 | 495 | 7.57×10$^{-5}$ | 2.24×10$^{-4}$ | 5.66×10$^{-5}$ |
| 60 | 5.6x10$^{-2}$ | 310 | 100 | 410 | 9.03×10$^{-5}$ | 2.80×10$^{-4}$ | 6.83×10$^{-5}$ |
| 70 | 5.6x10$^{-2}$ | 230 | 80 | 310 | 1.22×10$^{-4}$ | 3.50×10$^{-4}$ | 9.03×10$^{-5}$ |
| 80 | 5.6x10$^{-2}$ | 200 | 63 | 263 | 1.40×10$^{-4}$ | 4.44×10$^{-4}$ | 1.06×10$^{-4}$ |

Table S6 Ionic Conductivity of LLZO-3-PAN SSE

| T (℃) | d (cm) | $R_g$ (Ω) | $R_{gb}$ (Ω) | R (Ω) | σ ($R_g$)(S cm$^{-1}$) | σ ($R_{gb}$)(S cm$^{-1}$) | σ (R)(S cm$^{-1}$) |
|---|---|---|---|---|---|---|---|
| 25 | 5.5x10$^{-2}$ | 700 | 100 | 800 | 3.94×10$^{-5}$ | 2.76×10$^{-4}$ | 3.45×10$^{-5}$ |
| 30 | 5.5x10$^{-2}$ | 650 | 94 | 744 | 4.25×10$^{-5}$ | 2.94×10$^{-4}$ | 3.71×10$^{-5}$ |
| 40 | 5.5x10$^{-2}$ | 525 | 90 | 615 | 5.26×10$^{-5}$ | 3.07×10$^{-4}$ | 4.49×10$^{-5}$ |
| 50 | 5.5x10$^{-2}$ | 385 | 60 | 445 | 7.17×10$^{-5}$ | 4.60×10$^{-4}$ | 6.20×10$^{-5}$ |
| 60 | 5.5x10$^{-2}$ | 310 | 55 | 365 | 8.90×10$^{-5}$ | 5.02×10$^{-4}$ | 7.56×10$^{-5}$ |
| 70 | 5.5x10$^{-2}$ | 235 | 50 | 285 | 1.17×10$^{-4}$ | 5.52×10$^{-4}$ | 9.68×10$^{-5}$ |
| 80 | 5.5x10$^{-2}$ | 203 | 43 | 246 | 1.36×10$^{-4}$ | 6.42×10$^{-4}$ | 1.12×10$^{-4}$ |

Table S7 performance comparison of garnet-based LLZO solid-State electrolytes

| SSEs | σ(mS cm$^{-1}$) | electrochemical Window (V) | cathode | initial capacity (mAh g$^{-1}$) | Ref. |
|---|---|---|---|---|---|
| PVDF-HFP/LLZO | 2.8×10$^{-4}$ | 4.29 | LFP | 162 (0.2C) | [1] |
| 20%LLZO/SB-PVDF/LiTFSI | 1.73×10$^{-4}$ | 5.22 | LFP | 138.2 (0.5C) | [2] |
| Al-doped LLZO/PVDF | 1.16×10$^{-4}$ | / | NCA | 213(0.2C) | [3] |
| LLZTO/PEO | 1.1×10$^{-4}$ | 4.8 | LFP | 152.3(0.5C) | [4] |
| Li$_{6.6}$La$_{2.8}$Mg0.2Zr$_{1.4}$Ta$_{0.6}$O$_{12}$ | 4.31×10$^{-4}$ | / | NCM622 | 140 (0.1C) | [5] |
| PL-LILZO NFs(0.2) | 9.39×10$^{-4}$ (at 60 ℃) | 5.2 | LFP | 136(0.5C) | [6] |
| PDA@LLZTO | 4×10$^{-4}$ | 4.8 | LFP | 146.9(0.5C) | [7] |
| LLZTO-based film | 1.05×10$^{-4}$ （30℃） | 4.6 | LFP | 153(0.1C,60℃) | [8] |
| LLZO-PAN | 1.11×10$^{-4}$ | 4.29 | LFP | 256.2(0.1C) | This work |

Ionic conductivity depends on the charge mobility and charge carrier concentration, while activation energy ($E_a$) reflects charge mobility. $E_a$ was calculated using Eq. (S2).

$$\sigma = A exp(-E_a/K_B T) \qquad (S2)$$

where σ represents the ionic conductivity of the analyzed samples, $A$ indicates the prefactor, $T$ denotes the testing temperature, $K_B$ represents the Boltzmann constant, and $E_a$ refers to the activation energy of the samples.
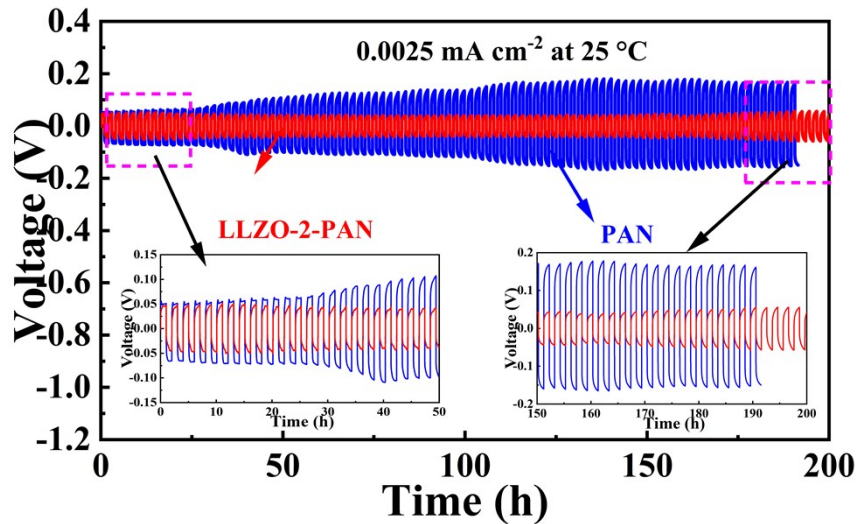
Fig. S5 Voltage profiles of Li‖Li symmetric half-cell with the PAN and LLZO-2-PAN composite electrolyte.

Fig. S6 illustrates the SEM image and optical photograph of the LLZO-2-PAN composite electrolyte. Fig. S6(a) depicts the SEM image of the LLZO-2-PAN composite electrolyte prior to the cycling process. It can be observed that the LLZO-2 particles are distributed homogeneously throughout the PAN matrix. Fig. S6(b) depicts the SEM image of the LLZO-2-PAN composite electrolyte following the completion of the cycling process. It is evident that the LLZO-2 particles are dispersed in a uniform manner within the PAN matrix. Fig. S6(c) depicts the SEM image of the LLZO-2-PAN composite electrolyte following the completion of the cycling process. Fig. S6(d,e,f) depicts the optical photographs of the LLZO-2-PAN composite electrolyte, both in its original state and following the completion of the cycling process. As evidenced by the photographs, the physical properties of the LLZO-2-PAN composite electrolyte remained unaltered prior to and following the electrochemical reaction. The SEM images and optical photographs of the LLZO-2-PAN composite electrolyte, taken before and after electrochemical cycling, revealed that no chemical reaction occurred, such as decomposition of LLZO-2, during the electrochemical cycling process.
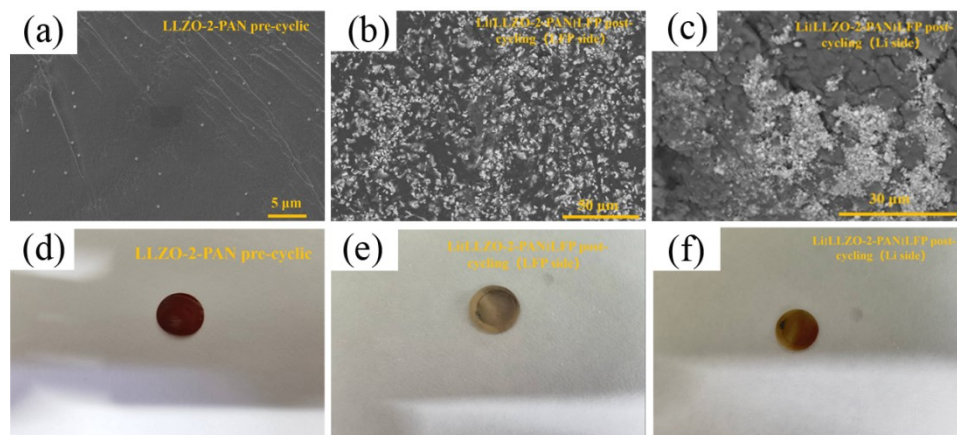


Fig. S6 LLZO-2-PAN composite electrolyte pre-cyclic of (a) SEM image, LLZO-2-PAN composite electrolyte post-cycle of (b) SEM image (LFP side), (c)SEM image (Li side), (d) LLZO-2-PAN composite electrolyte pre-cyclic of optical photograph; LLZO-2-PAN composite electrolyte post-cycle of (e) optical photograph (LFP side) (f).optical photograph (Li side).

As an inorganic active filler, oxygen-deficient LLZO is a promising fast lithium-ion conductor with high room temperature ionic conductivity and intrinsic stability to lithium metal. To investigate the chemical stability of LLZO-2 in Li‖LLZO-2-PAN‖LFP all-solid-state batteries pre-cycling and post-cycling the electrochemical reaction, XPS tests were performed on the LLZO-2-PAN composite electrolyte before and after the electrochemical reaction. Fig. S7 presents the XPS spectra of LLZO-2 (pre-cycling) and LLZO-2-PAN composite electrolyte (Li‖LLZO-2-PAN‖LFP post-cycling). The results show that the elements Li, Zr, La, and O can be detected both before and

after the reaction, and that the valence and binding energy of these elements remain unchanged. Compared to the initial state, the peak of intensity LLZO-2-PAN was reduced after the electrochemical reaction.
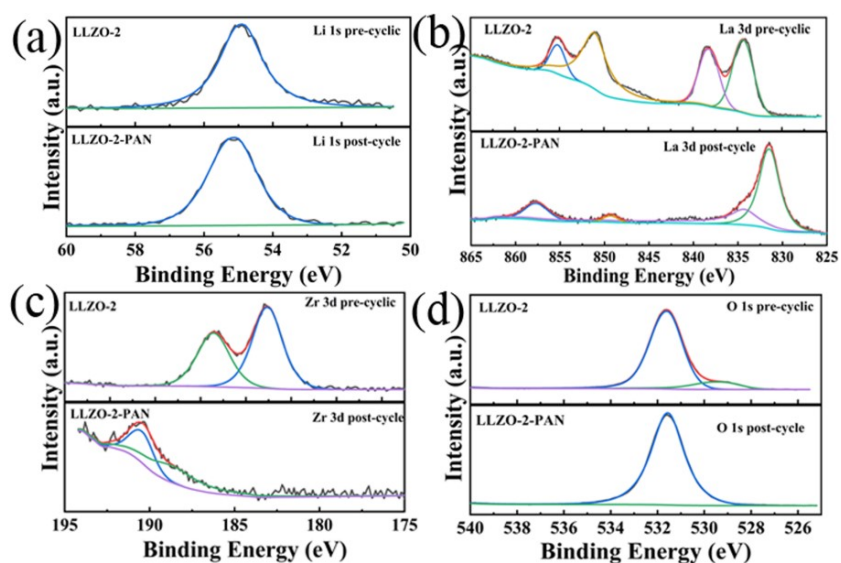


Fig. S7. XPS spectra of LLZO-2 (pre-cyclic) and LLZO-2-PAN (post-cycle)
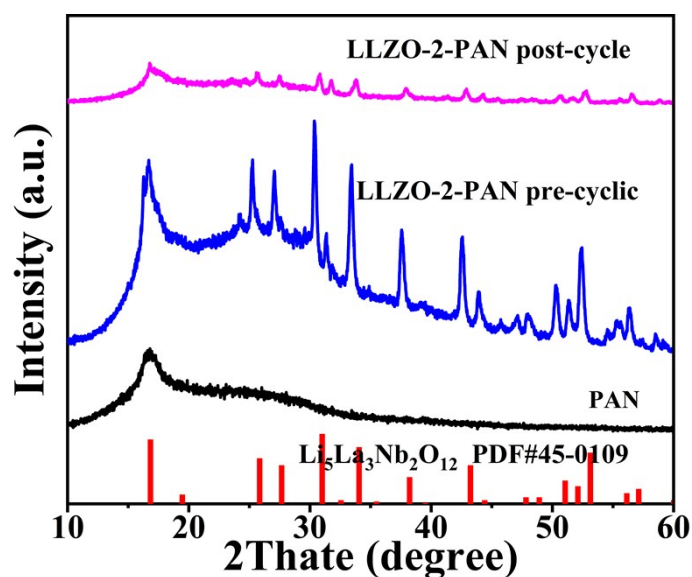(a) Li 1s, (b) La 3d, (b) Zr 3d, (c) O 1s.



Fig. S8 The XRD patterns of LLZO-2-PAN pre-cycle and post-cycle electrochemical cycling

Fig. S8 shows the XRD spectra of LLZO-2-PAN before and after electrochemical cycling. The solid state battery Li|LLZO-2-PAN|LFP before and after electrochemical cycling. The XRD spectra of the LLZO-2-PAN composite electrolyte were consistent with the standard $Li_5La_3Nb_2O_{12}$ map (PDF#45-0109). After 5 cycles, the intensity of the characteristic XRD diffraction peaks of LLZO-2-PAN becomes weaker and broader, which may be due to the deterioration of the crystallinity of the composite electrolyte after electrochemical cycling. Therefore, the LLZO-2-PAN composite electrolyte only provides a channel for lithium ions during the electrochemical process and no chemical reaction takes place.

**References**

1   Z. Fang, M. Zhao, Y. Peng, S. Guan, *ACS Appl. Mater. Interfaces,* 2022, **14**, 18922-18934.

2   H. Hou, B. Huang, X. Yu, J. Lan, S. Ming, J. Rong, X. Liu, F. Chen, *Journal of Energy Storage,* 2023, **68**, 1-10.

3   X. Ping, Q. Zheng, B. Meng, W. Lin, Y. Chen, C. Fang, H. Zhang, W. Liang, *Ceram. Int.,* 2022, **48**, 1-9.

4   Q. Guo, F. Xu, L. Shen, Z. Wang, J. Wang, H. He, X. Yao, *J. Power Sources,* 2021, **498**, 1-8.

5   K. Ma, B. Chen, C. Li, V. Thangadurai, *Advanced Sustainable Systems,* 2024, **8**, 1-13.

6   Y. Teng, H. Liu, Q. Wang, Y. He, Y. Hua, C. Li, J. Bai, *Journal of Energy Storage* 2024, **76**, 1-10.

7   Y. Wang, Z. Chen, Y. Wu, Y. Li, Z. Yue, M. Chen, *ACS Appl. Mater. Interfaces,* 2023, **15**, 21526-21536.

8   J. Huang, Y. Huang, Z. Zhang, H. Gao, C. Li, *Energy Fuels,* 2020, **34**, 15011-15018.